

Natural convection and pattern interaction in a two-dimensional vertical slot

J.M. Floryan^{1,†}, W. Wang¹, S. Panday¹ and Andrew P. Bassom²

¹Department of Mechanical and Materials Engineering, The University of Western Ontario, London, Ontario, N6A 5B9, Canada

²School of Natural Sciences, University of Tasmania, Private Bag 37, Hobart, TAS 7001, Australia

(Received 18 December 2021; revised 30 May 2022; accepted 29 June 2022)

Laminar natural convection is investigated in an infinite vertical slot which has one wall with a corrugated profile, and which is subject to either a uniform or periodic heating profile. This configuration has the attractive feature that it enables a study of the effects that may be produced via the interaction of heating and topography patterns. It is found that the addition of the grooves to an isothermal plate leads to a reduction in the vertical fluid flow and an increase of the transverse heat flow. In contrast, imposing sinusoidal heating on a flat surface generates convection that appears as counter-rotating rolls but there is no net vertical flow. The combination of the two effects of corrugation together with periodic heating leads to a plethora of flow patterns involving a combination of rolls and stream tubes that carry the fluid along the slot. The details of this vertical flow are governed by a pattern interaction effect dictated by the relative positions of the heating and corrugation patterns; when hot spots of the imposed heating overlap the peaks in the grooves the net flow is upward; in contrast, when they lie over the troughs the resultant flow is downward. The interplay between the thermal and geometrical effects weakens as the wavelength of the structure is reduced. The inclusion of a sufficiently strong uniform heating also seems to wash away the pattern interaction effect.

Key words: convection

1. Introduction

Natural convection in vertical openings is of interest in architectural design as it provides the means for passive ventilation through the so-called stack effect, whereby heated air flows in the upward direction and draws in cool air at the base of a structure (Linden 1999; Wong & Heryanto 2004; Nagler 2021). A reverse stack effect can also occur in which relatively hot air is brought down from above into a cooler environment. Vertical

† Email address for correspondence: floryan@uwo.ca

openings are also of importance in the design of various fire prevention measures owing to the possibility of controlling the intensification of combustion and the spreading of fires (Song *et al.* 2020). Upright fault lines are known to be significant in the context of thermal recovery processes (Tournier, Gethon & Rabinowicz 2000). Convection can be used for cooling by arranging hot surfaces to form vertical slots – this process is known as the chimney effect, a name coined from the first type configuration used to remove smoke from fireplaces (Putnam 1882). More contemporary uses of the chimney effect include the passive cooling of electronic components (Naylor, Floryan & Tarasuk 1991; Straatman, Tarasuk & Floryan 1993; Straatman *et al.* 1994; Novak & Floryan 1995; Shahin & Floryan 1999; Andreozzi, Buonomo & Manca 2005) as well as in the design of passively cooled nuclear reactors (Weil 2012).

Fundamental studies of vertical natural convection can be traced back to Zeldovich (1937), who developed the theory for self-similar, laminar plane and axisymmetric plumes, and to Batchelor (1954), who considered a closed vertical cavity. Subsequent studies have been focused on the possible transition to secondary states (Vest & Arpaci 1969; Lee & Korpela 1983; Hall 2012), and on turbulent convection (Ng *et al.* 2015) and the effect of roughness (Shishkina & Wagner 2011; Toppaladoddi, Succi & Wettlaufer 2017). Further work has examined the modifications created by ratchet surfaces (Jiang *et al.* 2019). All these studies typically involved bounding surfaces kept at prescribed uniform temperatures.

A more recent direction in convection research involves the use of patterned heating (Hossain & Floryan 2013, 2015a) in which the temperature of the boundaries is not constant, but rather it adopts some form of prescribed spatial structure (Hughes & Griffiths 2008). Most of the results available are restricted to horizontal slots and demonstrate similarities in the system response regardless of whether the heating is applied from above or below (Hossain & Floryan 2014, 2015b). Transition to secondary states is driven by a competition between the spatial parametric resonance and the Rayleigh–Bénard (RB) mechanism (Bénard 1900; Rayleigh 1916; Hossain & Floryan 2013) and often exhibits a strong dependence on the Prandtl number Pr . The use of isothermal corrugated surfaces leads to a different type of convection which represents a forced response rather than a bifurcation as in the case of RB convection and exhibits Pr dependence (Abtahi & Floryan 2017a). The combination of heating and topography patterns activates the interaction mechanism (Floryan & Inasawa 2021), which leads to thermal drift (Abtahi & Floryan 2017b, 2018; Inasawa, Hara & Floryan 2021). It is known that patterned heating can lead to a reduction in the pressure losses along a horizontal conduit (Hossain, Floryan & Floryan 2012; Floryan & Floryan 2015; Hossain & Floryan 2016) as well as a weakening in the driving force in the case of the relative motion between two plates (Floryan, Shadman & Hossain 2018). The combination of heating and groove patterns may conceivably lead to a reduction in pressure losses greater than can be achieved by pure heating alone (Hossain & Floryan 2020). This opens the door to the opportunity for the development of flow control techniques based on carefully setting the relative positions of the heating elements and the corrugations in the surface.

With this possibility in mind, this paper is focused on the analysis of natural convection in vertical slots driven by patterned heating and modified by surface grooves. One side of the slot is smooth and isothermal while the other is corrugated and subject to a combination of periodic and uniform heating. It is important to emphasize at this early juncture that our concern is with laminar flow. Turbulent situations are undoubtedly possible with sufficiently strong heating, as evidenced by the work of Ng *et al.* (2015). They demonstrated that flows which exhibit the chimney effect can be laminar-like or turbulent.

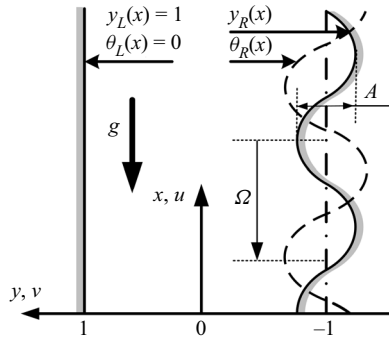


Figure 1. Schematic diagram of the flow system.

We begin our study in § 2, which provides a description of the model problem. The next few sections of the paper are devoted to a description of the numerical results and focus on various aspects of the flow. In § 3 we concentrate on the effect of the geometry of the wall and so consider the flows that are generated when the amplitude of the grooves is varied while the temperature of wall is uniform. In § 4 we introduce periodic heating to the grooved wall; it is found that, under certain circumstances, stream tubes may be created. We combine the uniform and periodic heating components in § 5 and discuss the modifications that ensue. In § 6 we consider a long-wavelength analysis of the problem which helps confirm some of the preceding numerical findings. We round off the paper with some final remarks and discussion.

2. Problem formulation

Consider an infinite vertical slot formed by one smooth and one corrugated plate as sketched in figure 1; the coordinate axes are such that the positive x -axis points upwards, and the y -axis is directed from right to left. The geometry of the slot is then given by

$$y_L(x) = 1, \quad y_R(x) = -1 + \frac{1}{2}A \cos(\alpha x), \tag{2.1a,b}$$

where the subscripts L, R refer to the left and right plates, and we have non-dimensionalized lengths on half the mean slot opening h . We remark that the left edge of the slot is flat, while the other boundary is corrugated; the grooves are of peak-to-trough amplitude A and of wavenumber α or, equivalently, of wavelength

$$\lambda = 2\pi/\alpha. \tag{2.2}$$

The left plate is supposed to be isothermal while the right boundary is subject to an imposed heating which is partly uniform and partly periodic in space. This implies that on the sides of the slot the two temperature distributions are given by

$$\theta_L(x) = 0 \quad \text{and} \quad \theta_R(x) = Ra_{uni} + \frac{1}{2}Ra_{p,R} \cos(\alpha x + \Omega), \tag{2.3a,b}$$

where θ denotes the associated temperature field. This is defined to be $\theta = T - T_L$ where the temperature of the left plate T_L is used as a reference level and θ has been scaled on $\kappa\nu/(g\Gamma h^3)$; here g is the gravitational acceleration, Γ denotes the thermal expansion coefficient, ν is the kinematic viscosity and κ the thermal diffusivity.

We emphasize the presence of the phase angle Ω which allows us to examine a heating pattern which is offset relative to the underlying groove geometry. The temperature of the

right boundary of the slot is dictated by the values of two appropriate Rayleigh numbers; Ra_{uni} sets the intensity of the uniform heating component while $Ra_{p,R}$ measures the size of the periodic modulations. The heating and groove patterns are perfectly tuned as they are characterized by identical wavenumbers.

Two-dimensional convection in the slot is governed by continuity, Navier–Stokes and energy equations written in the forms

$$\frac{\partial u}{\partial x} + \frac{\partial v}{\partial y} = 0, \quad u \frac{\partial u}{\partial x} + v \frac{\partial u}{\partial y} = -\frac{\partial p}{\partial x} + \nabla^2 u + Pr^{-1}\theta, \tag{2.4a,b}$$

$$u \frac{\partial v}{\partial x} + v \frac{\partial v}{\partial y} = -\frac{\partial p}{\partial y} + \nabla^2 v \quad \text{and} \quad u \frac{\partial \theta}{\partial x} + v \frac{\partial \theta}{\partial y} = Pr^{-1}\nabla^2 \theta. \tag{2.4c,d}$$

In this system (u, v) denote the velocity components in the (x, y) directions, respectively, scaled with $U_v = v/h$ while p is the pressure relative to the hydrostatic component and scaled on ρU_v^2 . The parameter $Pr = \nu/\kappa$ is the Prandtl number and in the subsequent computations we take $Pr = 0.71$, the value appropriate for air, unless stated otherwise.

The system of (2.4) needs to be solved subject to suitable flow and temperature constraints. We demand no slip on the sides of the slot so that

$$u(x, 1) = u(x, y_R) = 0, \quad v(x, 1) = v(x, y_R) = 0, \quad \theta(x, 1) = 0, \quad \theta(x, y_R) = \theta_R(x), \tag{2.5}$$

where y_R is defined in (2.1b) and the temperature profile $\theta_R(x)$ is given by (2.3b). We close the specification of the problem by noting that the solution must be periodic in x (with a periodicity dictated by the heating and groove patterns) and there is no externally imposed mean pressure gradient acting along the slot, i.e.

$$\left. \frac{\partial p}{\partial x} \right|_{mean} = 0. \tag{2.6}$$

The system (2.4)–(2.6) was solved by expressing the velocity components using the streamfunction ψ defined in the usual manner so that $u = \partial\psi/\partial y$ and $v = -\partial\psi/\partial x$. The pressure is eliminated between (2.4b,c) and the unknowns written in the form of Fourier expansions in the x -direction combined with Chebyshev expansions in the y -direction; this ensures that x -periodicity conditions are automatically satisfied.

The main computational challenge is posed by the irregularity of the solution domain and the need to consider the wide spectrum of geometries that can arise from the variations in the groove wavenumber and amplitude. There are various strategies that have been suggested to tackle this type of problem, and we chose to adopt a device known as the immersed boundary conditions method. The ideas underpinning this strategy are as follows. The computational domain is fixed, and the specific flow domain is then immersed within it. The discretized flow equations remain unchanged across all geometries and are solved simultaneously both inside and outside of the flow domain, but always so that the region remains inside the larger computational region. The flow boundaries are also located inside the computational domain and the flow conditions at these boundaries are posed as constraints (Szumbarski & Floryan 1999; Husain, Szumbarski & Floryan 2009; Husain & Floryan 2010) which are implemented using the tau method. This formulation circumvents the need for the numerical construction of intricate grids that replicate the groove geometry, a process which can be very labour intensive and error prone, and sidesteps the need for delicate grid convergence studies. All the elements of the discretization have spectral accuracy, so the global accuracy of the computations

is controlled by changing the number of Fourier modes and Chebyshev polynomials appropriately. All results presented in this paper were obtained with an accuracy of at least four digits. The groove shape is encoded within the algorithm by means of appropriate Fourier expansions which means that variations of groove geometry can be accounted for by simply changing the various coefficients.

A few important quantities can be used to monitor the properties of the flow. The first of these is the net vertical flow rate Q which is defined by

$$Q = \int_{y_R(x)}^1 u(x, y) dy. \tag{2.7a}$$

Useful measures of the heat transfer are provided by the local Nusselt numbers at the right (Nu_R) and left (Nu_L) plates. These are simply given by the appropriate normal derivatives $\partial\theta/\partial n$ so that on the two walls we have

$$Nu_R = - \left[1 + \frac{1}{4} \alpha^2 A^2 \sin^2(\alpha x) \right]^{-1/2} \left[\frac{1}{2} A \alpha \sin(\alpha x) \frac{\partial\theta}{\partial x} + \frac{\partial\theta}{\partial y} \right]_{y_R} \quad \text{and} \quad Nu_L = - \frac{\partial\theta}{\partial y} \Big|_{y_L}. \tag{2.8a,b}$$

These local values can be spatially averaged over the wavelength $\lambda = 2\pi/\alpha$ thereby giving a mean value

$$Nu_{av} = -\lambda^{-1} \int_0^\lambda \frac{\partial\theta}{\partial y} \Big|_{y_L} dx = -\lambda^{-1} \int_0^\lambda \left[\frac{1}{2} A \alpha \sin(\alpha x) \frac{\partial\theta}{\partial x} + \frac{\partial\theta}{\partial y} \right]_{y_R} dx, \tag{2.8c}$$

we remark that, necessarily, these values must be the same irrespective of which edge of the slot is used. This property was used as a check on the veracity of the computational work. For the analytical studies that we describe later it is evidently easier to evaluate Nu_{av} using values on the flat left-hand side of the slot. We also point out that a positive value of Nu_{av} implies that the left plate is gaining energy.

3. Isothermal plates

We commence our discussion of the properties of the induced convection when the two edges of the slot are isothermal so that the periodic part of the imposed heating is turned off ($Ra_{p,R} = 0$). Thus, we have an imposed uniform heating on the right-hand side of the slot together with any effects induced geometrically by the presence of the grooves.

Of course, when there is no corrugation, so $A = 0$, the governing equations admit a very simple exact solution in which the temperature, the streamwise velocity, the flow rate and the transverse heat flow are given by

$$\theta_S = \frac{Ra_{uni}}{2} (1 - y), \quad u_S = \frac{Ra_{uni}}{4} Pr^{-1} \left(\frac{1}{3} y - 1 \right) (y^2 - 1), \quad Q_S = \frac{Ra_{uni}}{3} Pr^{-1}, \quad Nu_{av,S} = \frac{1}{2} Ra_{uni}; \tag{3.1a-d}$$

here, the subscript S denotes that the various fields are associated with a smooth slot. We can conclude from these expressions that if $Ra_{uni} > 0$ the system undergoes heating, and the fluid moves upwards; conversely if $Ra_{uni} < 0$ there is cooling and downward motion.

Now we consider the introduction of the grooves so that $A \neq 0$. The results are presented in several complementary ways, and these are summarized in [figure 2](#). Here, we consider the flow rate Q and the average Nusselt number Nu_{av} relative to their respective values Q_S and $Nu_{av,S}$ in the absence of grooves. We take as a base case the flow when $Ra_{uni} =$

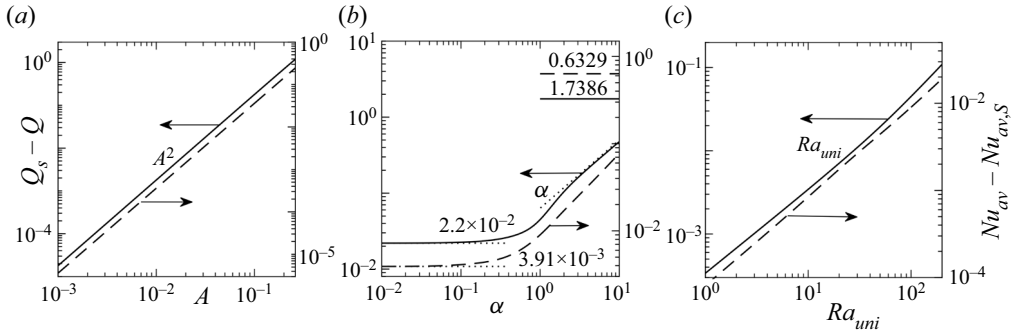


Figure 2. Variations of the reduction in the flow rate $Q_s - Q$ (solid line) and the increase of the heat flow $Nu_{av} - Nu_{av,S}$ (dashed line). Calculations were initially performed with the groove amplitude $A = 0.05$, wavenumber $\alpha = 1$ and a Rayleigh number $Ra_{uni} = 100$. The three plots show the effects of changing (a) the amplitude A , (b) the wavenumber α and (c) Ra_{uni} away from the initial state. The horizontal lines in the upper right corner in (b) denote the limits achieved as $\alpha \rightarrow \infty$.

100, the wavenumber $\alpha = 1$ and the groove amplitude $A = 0.05$ and then in figure 2 consider the effects of varying the groove amplitude, the wavenumber and Ra_{uni} separately. The results shown in figure 2(a) suggest that $Q_s - Q$ and $Nu_{av} - Nu_{av,S}$ increases are proportional to A^2 , at least over the range of groove sizes examined. In contrast, the effects of varying the groove wavenumber are somewhat more complex. There is a well-defined limit as $\alpha \rightarrow 0$ which can be determined using analysis that is deferred to § 6 below. As α increases, so $Q_s - Q$ and $Nu_{av} - Nu_{av,S}$ grow roughly proportional to α but this does not continue indefinitely; rather, there are upper bounds that are approached as α increases further. Last, we note that flux and heat transfer measures increase in proportion to Ra_{uni} (see figure 2c).

It is instructive to look at the various forces that act on the edges of the slot. The stresses on the plates can be ascribed to viscous and pressure forces. On the right-hand boundary the viscous part is

$$\sigma_{xv,R} = \left[-\alpha A \sin(\alpha x) \frac{\partial u}{\partial x} \Big|_{y_R} - \left(\frac{\partial u}{\partial y} + \frac{\partial v}{\partial x} \right) \Big|_{y_R} \right] \left[1 + \frac{1}{4} \alpha^2 A^2 \sin^2(\alpha x) \right]^{-1/2}, \quad (3.2a)$$

and the pressure part is

$$\sigma_{xp,R} = \frac{1}{2} \alpha A \sin(\alpha x) p|_{y_R} \left[1 + \frac{1}{4} \alpha^2 A^2 \sin^2(\alpha x) \right]^{-1/2}, \quad (3.2b)$$

and the corresponding mean forces ($F_{xv,R}$, $F_{xp,R}$) are obtained by spatially averaging over a wavelength. On the flat left-hand plate, the local viscous stress is simply

$$\sigma_{xv,L} = \frac{\partial u}{\partial y} \Big|_{y_L}, \quad (3.2c)$$

while $\sigma_{xp,L} = 0$ and the mean value $F_{xv,L}$ is defined in the natural way.

We note that in the case of no grooves in the right-hand plate we have

$$F_{xv,SR} = -\frac{2}{3} Ra_{uni} Pr^{-1}, \quad F_{xv,SL} = -\frac{1}{3} Ra_{uni} Pr^{-1}; \quad (3.3a,b)$$

again, the S designation reminds us that there are values associated with a smooth right-hand boundary.

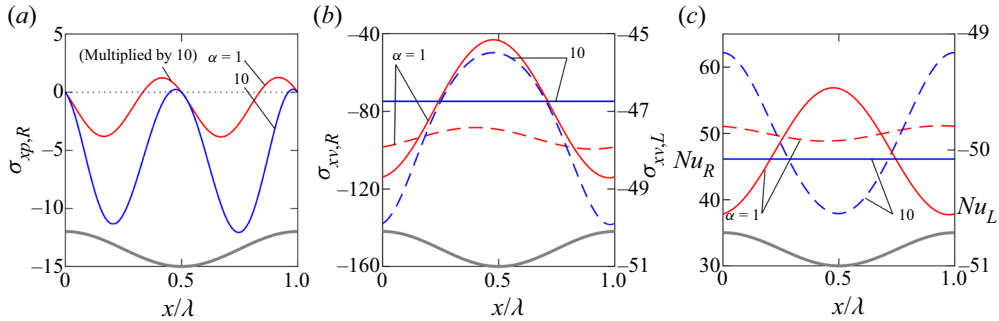


Figure 3. (a) The spatial distribution of the pressure force $\sigma_{xp,R}$ at the right plate for the parameter choices $Ra_{uni} = 100$, $A = 0.05$, $\alpha = 1$ (red lines) and $\alpha = 10$ (blue lines). In (b) are shown the x -components of the viscous forces at the right ($\sigma_{xv,R}$) and the left ($\sigma_{xv,L}$) plates shown by solid and dashed lines, respectively. The two local Nusselt numbers at the right (Nu_R) and left (Nu_L) plates are shown in (c) by solid and dashed lines respectively. The grey lines at the bottom of each figure denote the shape of the groove.

The results summarized in figure 3 suggest that the addition of grooves tends to add pressure resistance while decreasing the viscous component and this effect becomes increasingly pronounced at larger α . The distributions of the local heat fluxes as described by (2.8a,b) show that the heat flow tends to concentrate at the groove peaks. On the other hand, variations in the mean values Nu_{av} are minimal as the grooves are insufficiently powerful to generate significant transverse fluid movement.

4. Periodic heating

We now switch attention to the case when convection is driven by periodic heating and, once again, start with the situation without grooves. The flow is driven by the buoyancy force which switches direction every half-wavelength. The fluid flows upwards along the heated segment of the plate and downwards along the cooled section which gives rise to counter-rotating rolls with one pair per wavelength, as illustrated in figure 4(a). The downwards moving fluid meets the upwards moving fluid with pressure rising in the collision zone and reaching a maximum around $x = 0.25\lambda$ (see figure 4b) forcing the fluid to turn into the interior of the slot. The pressure minimum forms around $x = 0.75\lambda$ as the fluid is drawn by buoyancy force away from the plate. This pressure minimum draws the fluid from the interior of the slot. The pressure remains nearly constant in the horizontal direction, as illustrated in figure 4(b).

Typical velocity and temperature distributions are displayed in figure 5 and confirm the expectation that the temperature varies across the whole slot and the rolls fill the region when the heating wavenumber $\alpha = O(1)$. As α grows, we see the formation of a thermal boundary layer attached to the heated plate with the associated convection confined to this thin region (see figure 5b,c).

In fact, it is not difficult to describe the flow when α is large. Elementary scaling of the governing equations (2.4) shows that the flow is confined to an $O(\alpha^{-1})$ zone next to the right-hand wall and, if $y = -1 + \alpha^{-1}Y$ here, the leading-order temperature field is given by

$$\theta(x, Y) = \frac{1}{2}Ra_{p,R}exp(-Y) \cos \alpha x. \tag{4.1}$$

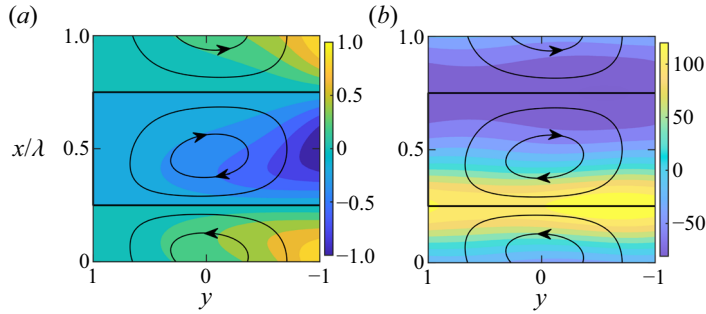


Figure 4. (a) The flow and temperature fields and (b) the flow and pressure fields for periodic heating in a slot with smooth sides. Parameter values are $Ra_{p,R} = 400$, $\alpha = 1$. Temperature has been normalized so that its maximum value is unity.

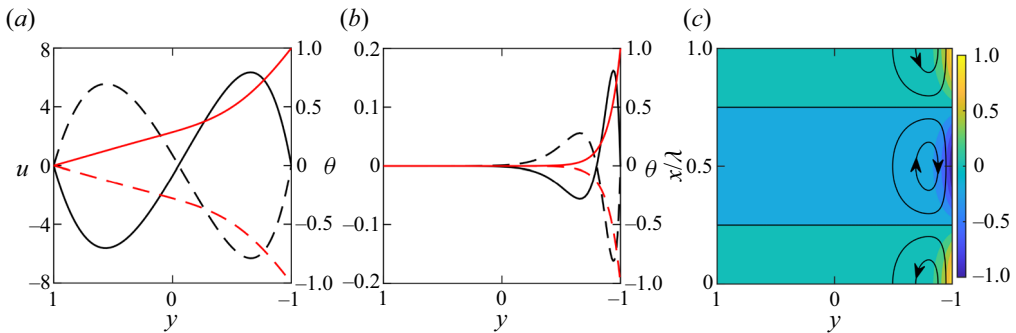


Figure 5. The distribution of the x -velocity component u (black lines, left axis) and the temperature θ (red lines, right axis) as functions of y at $x = 0$ (solid lines) and $x = \lambda/2$ (dashed lines) when $Ra_{p,R} = 400$: (a) $\alpha = 1$; (b) $\alpha = 10$; (c) the flow and the temperature fields associated with $\alpha = 10$.

This thermal profile drives a weak flow

$$u = -\frac{\alpha^{-2}}{16Pr} Ra_{p,R} Y(2 - Y) \exp(-Y) \cos \alpha x, \quad v = -\frac{\alpha^{-2}}{16Pr} Ra_{p,R} Y^2 \exp(-Y) \sin \alpha x, \tag{4.2a,b}$$

and we see how there is exponential decay as we leave the boundary layer.

The flow patterns change significantly when grooves are introduced. This is depicted in [figure 6](#) where we can see a stream tube that meanders between the rolls and transports fluid either upwards or downwards depending on the relative positioning of the imposed temperature hot spots and the groove peaks. When the hot spots are located close to the peaks, the stream tube is attached to the heated section of the groove and carries fluid upwards (see [figure 6a](#)). Conversely, when the hot spots are nearer to the groove troughs, the stream tube is adjacent to the cooled section of the groove and moves fluid downwards (see [figure 6c](#)). The maximum upward flow occurs when the phase shift is almost $\Omega = 0$, which corresponds to hot spots virtually coinciding with the groove peaks (see [figure 6a](#)) with the greatest downward flow occurring near $\Omega = \pi$. When the hot spots are positioned half-way between the groove peaks and troughs the stream tube is extinguished, as seen in [figure 6\(b,d\)](#).

As the heating pattern moves with respect to the grooves from $\Omega = 0$ through π and back to 2π the convection flow field evolves in the sequence shown in [figure 6\(a–d\)](#) while

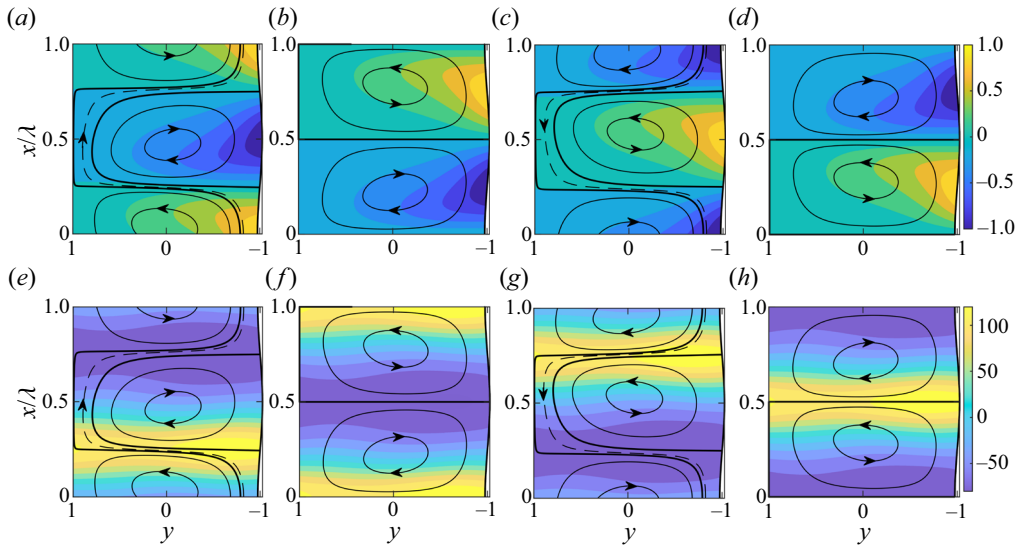


Figure 6. (a–d) The flow and the temperature fields and (e–h) the flow and pressure fields for the four phase angles $\Omega = 0, \pi/2, \pi$ and $3\pi/2$. The parameter values for the periodic heating are $Ra_{p,R} = 400$ and $\alpha = 1$ and the groove amplitude $A = 0.05$. Temperature has been normalized so that its maximum value is unity.

the pressure field development is described in figure 6(e–h). As the position of the pressure field moves relative to the grooves, so its projection onto the surface topography also changes, thereby producing a net surface pressure force that can be directed upwards (see, for example, figure 6e), downwards (figure 6g) or disappears completely (figure 6f,h). This is a manifestation of a pattern interaction effect (Floryan & Inasawa 2021) which is known to generate thermal drift in horizontal slots (Abtahi & Floryan 2017b; Inasawa *et al.* 2021).

The mechanism that controls the generation of the surface force is illustrated in detail in figure 7. The distributions of surface pressure at the heated plate displayed in figure 7(a) suggest how it shifts in the x -direction as the heating pattern moves. The projections of the surface pressure onto the topography generate an x -component of the pressure force which can be evaluated using equation (3.2b). Various distributions of $\sigma_{xp,R}$ are shown in figure 7(b). The surface pressure force is directed upwards nearly everywhere when $\Omega = 0$, downwards when $\Omega = \pi$, and averages to zero when $\Omega = \pi/2$ or $\Omega = 3\pi/2$. It is interesting to note that the choices $\Omega = \pi/2, 3\pi/2$ produce the largest flow rate in horizontal slots while $\Omega = 0, \pi$ generate no net flow (Abtahi & Floryan 2017b,c, 2018; Inasawa *et al.* 2021).

The above discussion summarizes how the flow is dictated by two processes; namely, the buoyancy force which acts within the fluid and the surface pressure force which works on the corrugated plate. Changes in the relative position of the hot spots with respect to the grooves result in a continuous variation in Q and Nu_{av} .

4.1. Convection with stream tubes

Unless the phase angle $\Omega = \pi/2$ or $3\pi/2$ the flow structure includes the emergence of stream tubes. At such values of Ω typical flow rates Q and mean Nusselt numbers Nu_{av} are proportional to both the groove amplitude A and the periodic Rayleigh number $Ra_{p,R}$ (see figures 8b and 8e). The dependence of these quantities on the wavenumber α is rather complex, as shown in figures 8(c) and 8(f) and requires closer inspection. Figure 8(c) suggests that the flow rate increases proportionally to α when α is greater than about one.

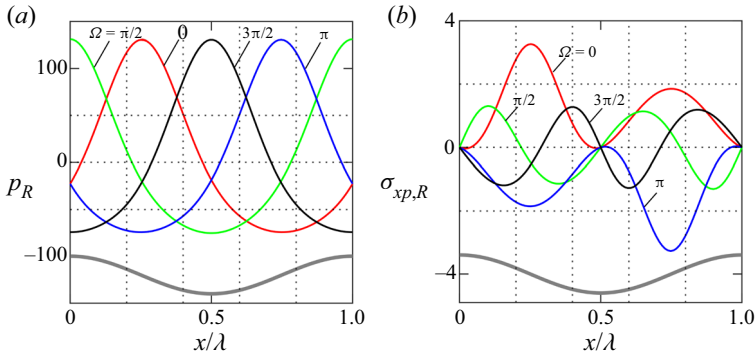


Figure 7. (a) The distribution of the surface pressure at the right plate p_R and (b) the x -component of the pressure force $\sigma_{xp,R}$ for the four phase angles Ω shown. The parameter values are $Ra_{p,R} = 400$, $Ra_{uni} = 0$, $\alpha = 1$, $A = 0.05$. The grey line at the bottom of each figure shows the shape of the groove.

This rise does not continue indefinitely – an upper bound on Q is furnished in the limit as $\alpha \rightarrow \infty$ when the groove peaks, which correspond to hot spots, bunch together – the plate behaves in a way not dissimilar to the situation that arises should the corrugated plate centred at $y = 1$ be replaced by an isothermal smooth plate located at $y = -1 + \frac{1}{2}A$ (i.e. at the peaks of the grooves) and held at a temperature $Ra_{uni} = \frac{1}{2}Ra_{p,R} = 200$. We also notice that at certain values of α the direction of the net flow switches. The heat flow also changes in a complicated way; it attains a local maximum near $\alpha = 1.5$ and there is a local minimum near $\alpha = 3$ (see figure 8f).

The forms of the flow and temperature fields for a selection of increasing values of α are illustrated in figure 9. When $\alpha = 1$ there are well-defined counter-rotating rolls which stretch between plates. As α increases towards 2 these rolls contract, with the structure near the left-hand plate being markedly reduced, see figure 9(a). This behaviour continues at α grows further (figure 9b), with the left rolls being eliminated completely once α reaches a value of 3. The right rolls persist but they too are barely visible once $\alpha = 5$ and are extinguished at $\alpha = 10$. The results shown in figure 8(c) suggest that the observed growth of Q roughly proportional to α begins near $\alpha = 2.48$, which correlates well with the value at which the rolls diminish. We suppose that at this juncture the corrugations in the grooved plate vary on a scale that is so small that the boundary begins to play a role more reminiscent of that of a smooth hot plate. The reduction in Nu_{av} apparent in figure 8(f) as α increases from 1.5 to approximately 3 corresponds to the gradual elimination of the rolls and the subsequent recovery and increase in Nu_{av} indicates onset of the dominance of conduction; this is very similar to what has been previously observed in the case of horizontal slots (Abtahi & Floryan 2017c). The structure of the temperature field clearly shows the formation of a thermal boundary layer near the heated plate as α grows; in contrast, the character of the flow field can be interpreted as the intensification of the stream tube as no velocity boundary layer appears.

Some details of the evolution of the flow and temperature fields are summarized in figure 10. As the wavenumber grows the process by which the thermal boundary layer is created is quite clear. The corresponding velocity field demonstrates a gradual elimination of downward movement when $\Omega = 0$ (and of upward motion should $\Omega = \pi$). It can be concluded that the preferred direction of motion obtained when the corrugations are of a short wavelength is set by the relative position of the heating and grooves.

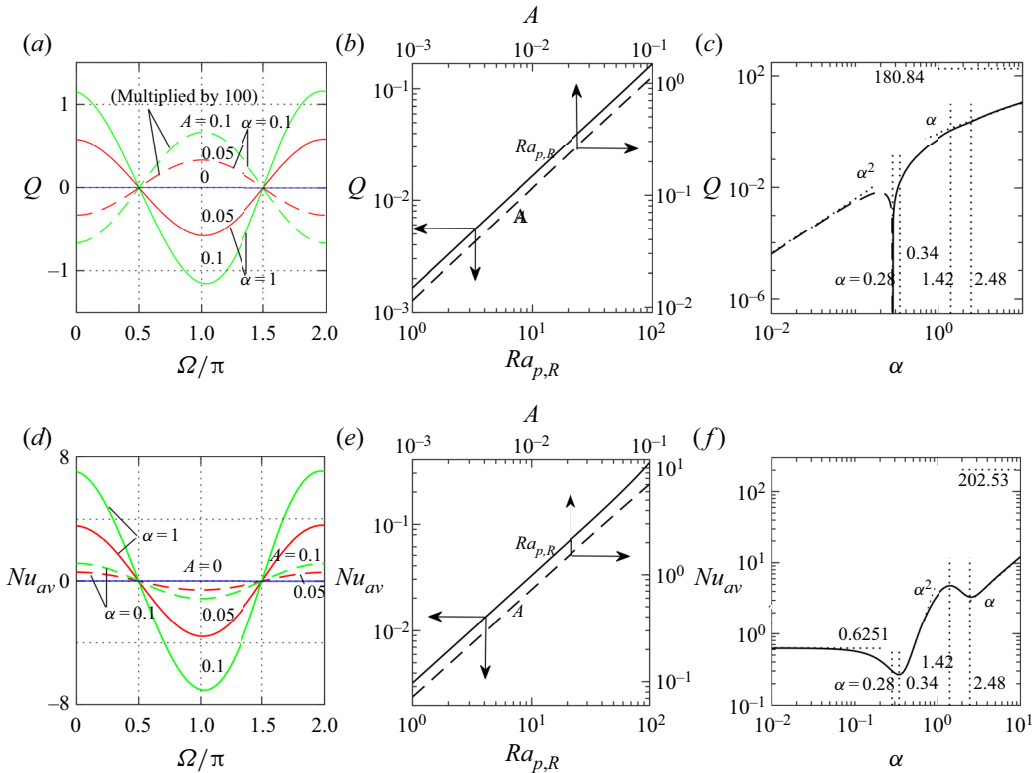


Figure 8. Flow characteristics for convection with periodic heating with $Ra_{p,R} = 400$, $\alpha = 1$, $A = 0.05$ and $\Omega = 0$. (a) The variations of the flow rate Q as a function of the phase difference Ω for the three amplitudes $A = 0, 0.05, 0.1$ and two wavenumbers $\alpha = 0.1$ and 1 . (b) Dependence of Q on the periodic Rayleigh number $Ra_{p,R}$ and the groove amplitude A and (c) on the groove wavenumber α with all the other parameters held fixed. The results for the average Nusselt number under the same flow conditions are shown in (d-f). The dashed lines on (c) denote a change in direction and the horizontal lines in the upper right corners of (c) and (f) denote the upper bounds for $\alpha \rightarrow \infty$.

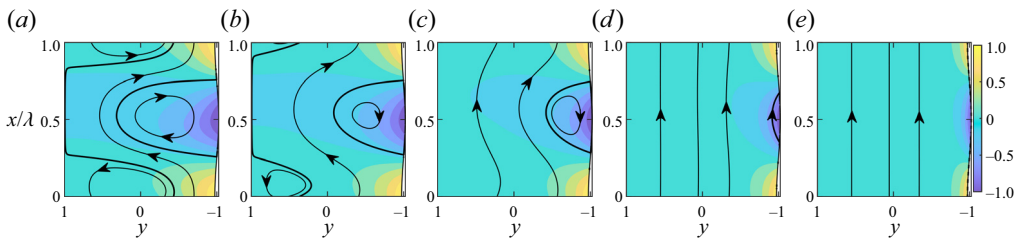


Figure 9. Convection properties for the parameter values $Ra_{p,R} = 400$, $A = 0.05$ and $\Omega = 0$. Shown are the flow and temperature fields for the five wavenumbers $\alpha = (a) 2, (b) 2.5, (c) 3, (d) 5$ and (e) 10 . Temperature has been normalized so that its maximum value is unity.

As α increases, the flow pattern becomes similar to that produced by a uniformly heated grooved slot while the pressure distribution on the surface of the heated plate replicates that in a flow through a grooved channel, see figure 11(a). The pressure acting on the fluid at the heated plate is positively contributing to the net driving force when $\alpha < \sim 9$ (see figure 11b). Further increase in α leads to elimination of the rolls and the upward

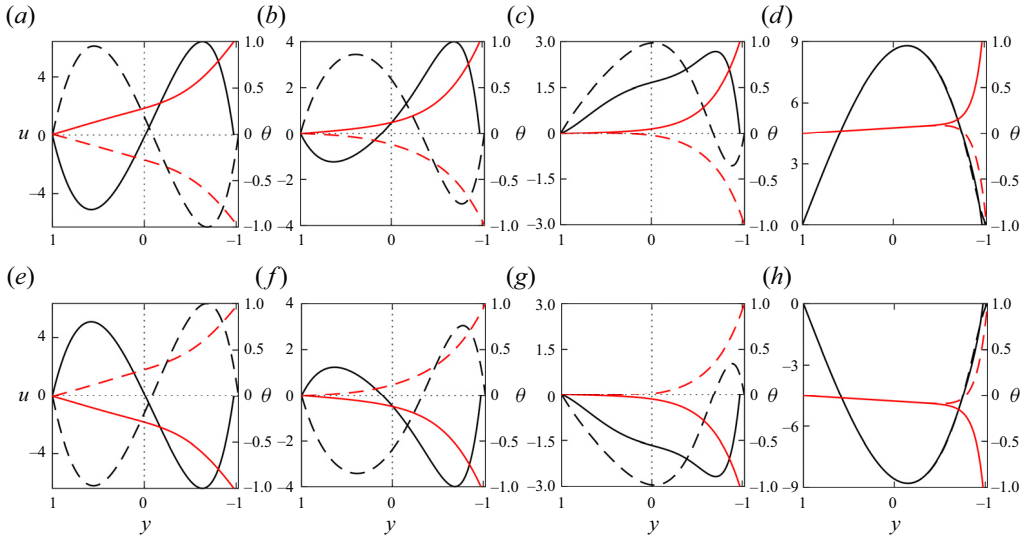


Figure 10. Distribution of the x -velocity component u (black lines, left axis) and of the temperature θ (red lines, right axis) as functions of y at $x = 0$ (solid lines) and $x = \lambda/2$ (dashed lines). Fields are shown for the four wavenumbers $\alpha = 1, 2, 3, 10$ and the two phase angles (a–d) $\Omega = 0$ and (e–h) $\Omega = \pi$. All results are for $Ra_{p,R} = 400$, $A = 0.05$ and temperature has been normalized so that its maximum value is unity.

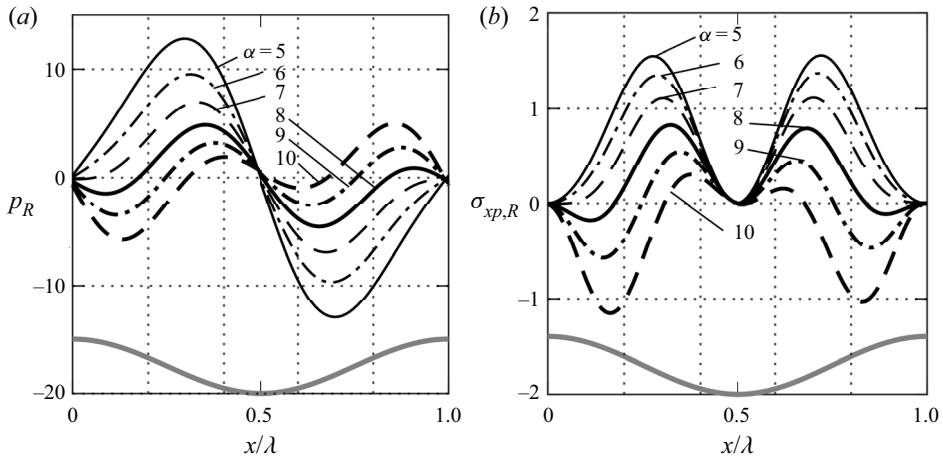


Figure 11. (a) The distribution of the surface pressure at the right plate p_R and (b) the x -component of the pressure force at the right plate $\sigma_{xp,R}$ when $Ra_{p,R} = 400$, $A = 0.05$ and $\Omega = 0$. Results are shown for the wavenumbers $\alpha = 5, 6, 7, 8, 9, 10$. The grey line at the bottom of each figure denotes the shape of the groove.

movement dominates the flow. Furthermore, the pressure force changes direction, and the grooves begin to play a role akin to that of roughness, thereby opposing the fluid movement (Mohammadi & Floryan 2013).

Next, we consider the long-wavelength limit $\alpha \rightarrow 0$. Once α falls below roughly 0.28 the direction of the stream tube switches (as shown in figure 8c) and it also moves and now is attached to the cooled section of the plate. The direction of the fluid transport is fixed by the value of the phase offset Ω . The pressure fields displayed in figures 6 and 12 are similar in as much that the x -components of the pressure forces are almost identical in

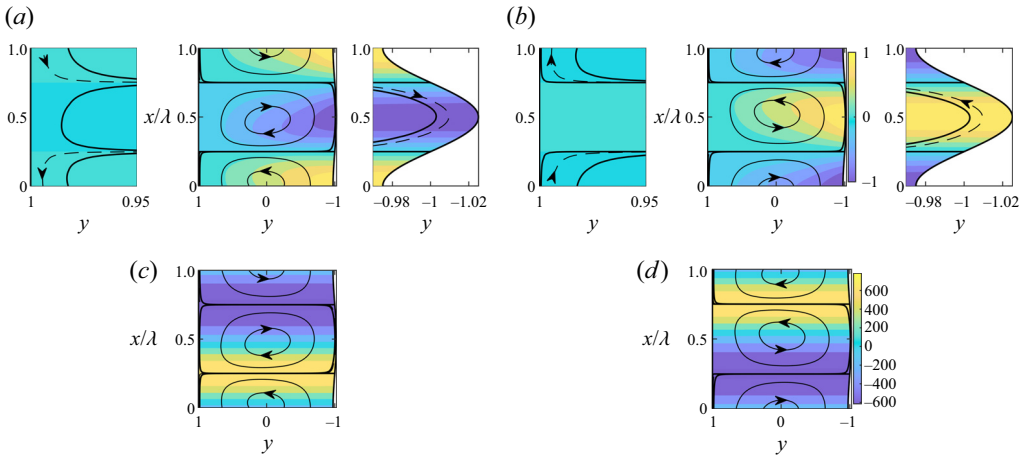


Figure 12. Convection solutions appropriate to the parameter choices $Ra_{p,R} = 400$, $\alpha = 0.2$ and $A = 0.05$. The flow and the temperature fields when (a) $\Omega = 0$ and (b) $\Omega = \pi$. The small figures either side of the central plots show enlargements of the zones near the respective plates. The flow and pressure fields associated with $\Omega = 0$ and $\Omega = \pi$ are shown in (c) and (d), respectively.

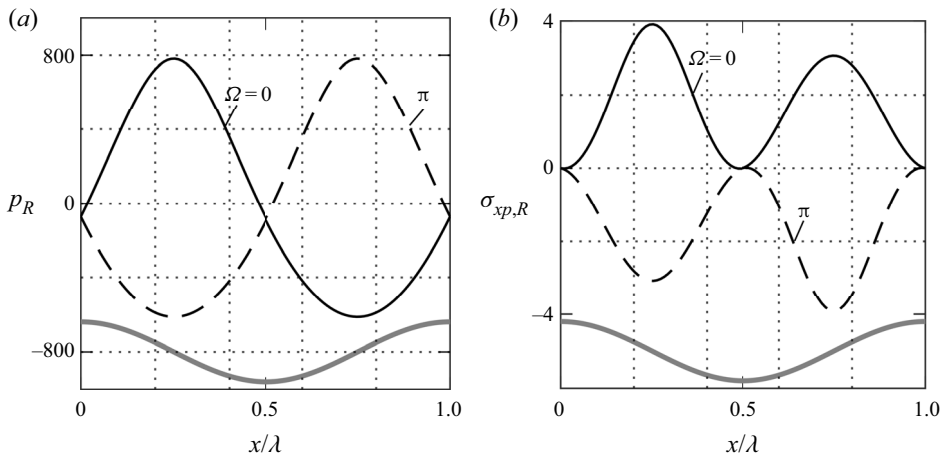


Figure 13. The distributions of (a) the surface pressure and (b) the x -component of the pressure force at the right plate when $Ra_{p,R} = 400$, $\alpha = 0.2$ and $A = 0.05$. Solid lines denote $\Omega = 0$ and dashed lines denote $\Omega = \pi$. The grey profile at the bottom of each figure represents shape of the groove.

the two cases (cf. figures 7 and 13) and the stream tube positions shown in figures 6 and 12 are kinematically consistent with the locations of the rolls. The only marked difference between the two flows is an order of magnitude increase in the pressure variations when α is small, but this in itself is insufficient to explain the change in the position of the stream tube. We conclude that it is the interplay between the buoyancy and the pressure forces which sets the location of the stream tubes and the direction of the flow within them; moreover, this changes as α decreases. Once the repositioning of the stream tube has occurred, any further reduction in α leads to a weakening of the overall flow field and the magnitude of Q diminishes proportional to α^2 (see figure 8c).

The evolution in Nu_{av} as α falls displays some interesting behaviour. With the particular parameter choices $Ra_{p,R} = 400$ and $A = 0.05$ it seems that over the range $0.34 < \alpha <$

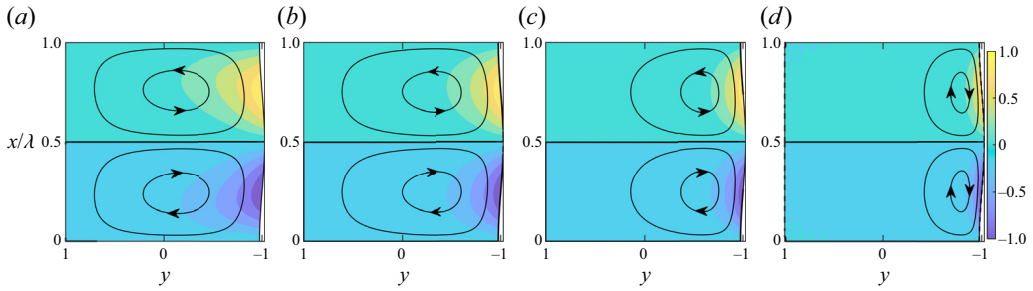


Figure 14. The flow and the temperature fields when $Ra_{p,R} = 400$, $Ra_{uni} = 0$, $A = 0.05$ and the phase offset $\Omega = \pi/2$. Shown are the fields for the four wavenumbers $\alpha = (a) 2$, $(b) 3$, $(c) 5$ and $(d) 10$. Temperature has been normalized so that its maximum value is unity.

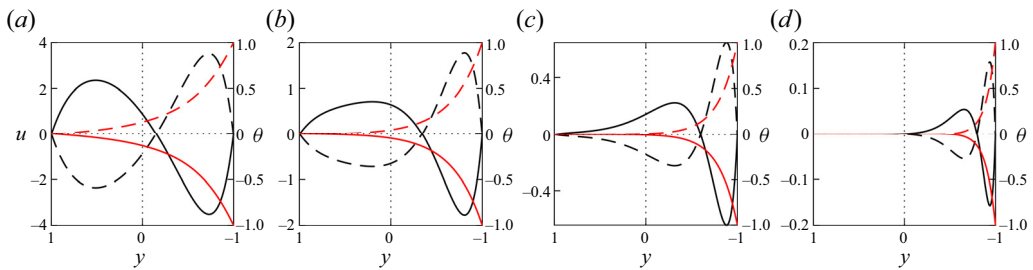


Figure 15. The distributions of the x -velocity component u (black lines, left axis) and the temperature θ (red lines, right axis) as functions of y at $x = \lambda/4$ (solid lines) and $x = 3\lambda/4$ (dashed lines) for the parameter values $Ra_{p,R} = 400$, $Ra_{uni} = 0$, $A = 0.05$ and the phase offset $\Omega = \pi/2$. Shown are the profiles for the four wavenumbers $\alpha = (a) 2$, $(b) 3$, $(c) 5$ and $(d) 10$. Temperature has been normalized so that its maximum value is unity.

1.42 the average Nusselt number roughly changes proportionally to α^2 . This behaviour can be ascribed to modifications in the intensity of the roll motion and the local minimum at around $\alpha = 0.34$ is associated with the complete elimination of the stream tube. Further reduction in α leads to the re-appearance of the stream tube (but on the opposite side of the rolls), an increase of Q and a concomitant rise in Nu_{av} . Eventually, this enhanced value in Q is arrested before the final $\alpha \rightarrow 0$ behaviour sets in. This sees a decrease in Q towards zero which is accompanied by Nu_{av} approaching a well-defined limit as $\alpha \rightarrow 0$ (figure 8f). This limit can be determined analytically, as explained in § 6 below.

4.2. Convection without stream tubes: the cases $\Omega = \pi/2$ and $\Omega = 3\pi/2$

The stream tubes are not formed for the two special cases when either $\Omega = \pi/2$ or $\Omega = 3\pi/2$. In these particular instances an increase in the wavenumber leads to the formation of both dynamic and thermal boundary layers near the heated plate. These features are clearly illustrated in figures 14 and 15, which demonstrate that all flow and thermal modulations are confined to these layers. These flows are distinctive compared with those patterns that arise at other values of Ω when stream tubes occur, and the only boundary layers are thermal in character. We also remark that both the flow and temperature fields are similar to those associated with convection in the case of a smooth slot exposed to periodic heating in the limit of $\alpha \rightarrow \infty$ (cf. figures 5 and 14).

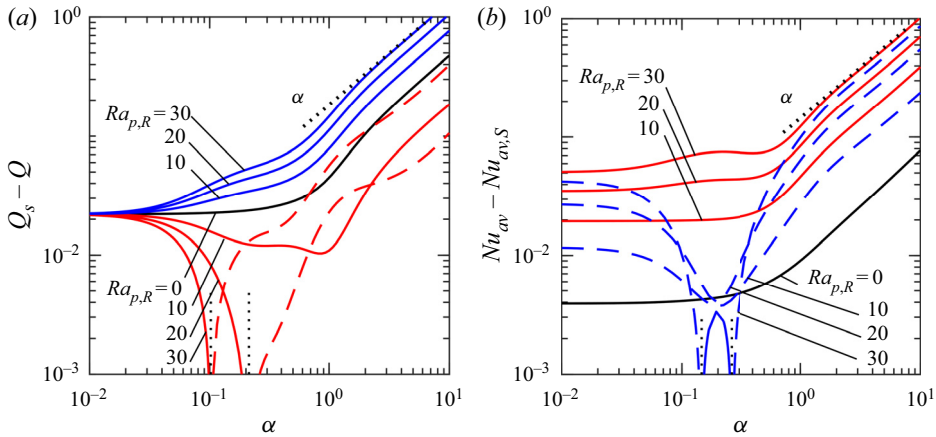


Figure 16. (a) Variations in the reduction of the flow rate $Q_s - Q$ and (b) the increase in the heat flow $Nu_{av} - Nu_{av,S}$ resulting from the introduction of grooves as functions of the groove wavenumber α . Computations performed for $A = 0.05$, $Ra_{uni} = 100$, $Ra_{p,R} = 10, 20, 30$ for $\Omega = 0$ (red lines) and $\Omega = \pi$ (blue lines). The black lines correspond to the results when $Ra_{p,R} = 0$ with all other parameters unchanged. Solid and dashed lines correspond to positive and negative values, respectively.

5. Corrugated slot exposed to a combination of periodic and uniform heating/cooling

We shall now discuss convection in a corrugated slot when the applied heating is a combination of uniform and periodic heating. We shall restrict the discussion to uniform heating as uniform cooling produces equal and opposite effects. We shall also focus attention on $\Omega = 0$ and $\Omega = \pi$ as effects of periodic heating change periodically as a function of Ω in the identical manner as was shown in figure 8(a). The results displayed in figure 16(a) illustrate the form of $(Q_s - Q)$ as a function of α – positive values mean that the flow rate is less than the reference flow rate. The inclusion of uniformly heated grooves reduces the flow rate as denoted by the black line in figure 16(a). A small component of periodic heating with the hot spots coincident with the groove peaks ($\Omega = 0$) increases this flow rate, which becomes larger than the flow rate in a smooth channel once $Ra_{p,R} > 10$. This increase becomes more pronounced at larger wavenumbers. Moving the hot spots to the groove troughs ($\Omega = \pi$) produces the opposite effect with an evident reduction in Q . Consideration of the distribution of the x -component of the surface pressure force acting on the fluid at the right plate shows that the total pressure force is negative for isothermal grooves as these tend to act as surface roughness thereby increasing the flow resistance (figure 17). The addition of periodic heating with hot spots at the groove peaks reduces the magnitude of this force due to the pattern interaction effect, which leads to an increase of Q . The variations in the mean Nusselt number tend to follow a similar behaviour. If hot spots are placed on the groove peaks this increases Nu_{av} but putting at the troughs decreases it and, furthermore, can even reverse the direction of the heat flow over a small range of α .

The effects of adding a small component of uniform heating to periodically heated grooves are illustrated in figure 18. The differences for small α are evident since $Q \rightarrow 0$ for periodic heating while $Q \rightarrow \text{const.}$ for uniform heating when $\alpha \rightarrow 0$. In these cases, the addition of even a small component of uniform heating drastically changes the response of the system (see figure 18a). At larger α the qualitative behaviour in many ways mimics what has been noted already in as much that uniform heating increases the flow rate when the hot spots overlap with the groove peaks but decreases it when they overlap with the

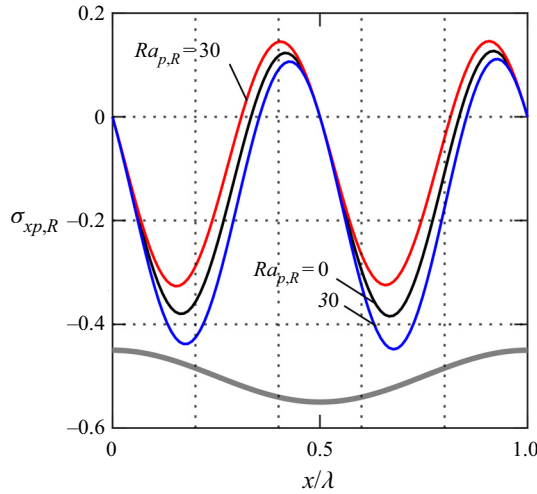


Figure 17. The structure of the x -component of the pressure force at the right plate when $Ra_{uni} = 100$, $\alpha = 1$, $A = 0.05$ for $\Omega = 0$ (red lines), and $\Omega = \pi$ (blue lines). The black line denotes the distribution for a purely uniform heating. The grey line at the bottom of the plot indicates the profile of the groove. The x -component of the total pressure force $F_{xp,R}$ for $\Omega = 0$ and $Ra_{p,R} = 0, 30$ is $-0.1287, -0.0901$, respectively; when $\Omega = \pi$ the corresponding results are $-0.1287, -0.1672$.

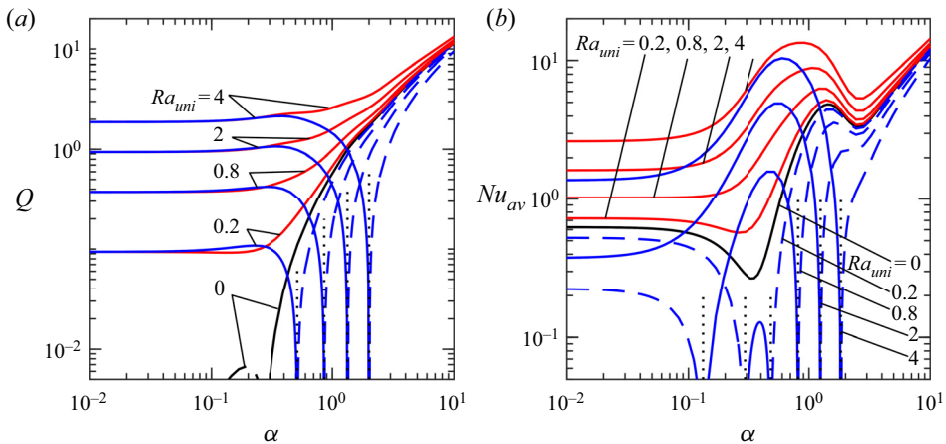


Figure 18. (a) Variations in the flow rate Q and (b) the average Nusselt number Nu_{av} as functions of the groove wavenumber α for $Ra_{p,R} = 400$, $\alpha = 1$, $A = 0.05$, $Ra_{uni} = 0, 0.2, 0.8, 2, 4$. Phase offset is set to be either $\Omega = 0$ (red lines) or $\Omega = \pi$ (blue lines). The black lines correspond to a purely periodic heating. Dashed lines indicate negative values.

troughs. The implications for Nu_{av} follow a similar pattern (cf. figures 16b and 18) but the changes at small α are less pronounced since $Nu_{av} \rightarrow \text{const.}$ as $\alpha \rightarrow 0$ regardless of the type of heating.

We now briefly discuss effect of the value of the Prandtl number. The flow rate increases proportionally to Pr^{-1} for a uniformly heated slot, as suggested by (3.1). The effect of the introduction of isothermal grooves changes the flow in a similar manner irrespective of the value of Pr and seems not to affect Nu_{av} at all. The main effects of varying Pr are summarized by the results given in figure 19.

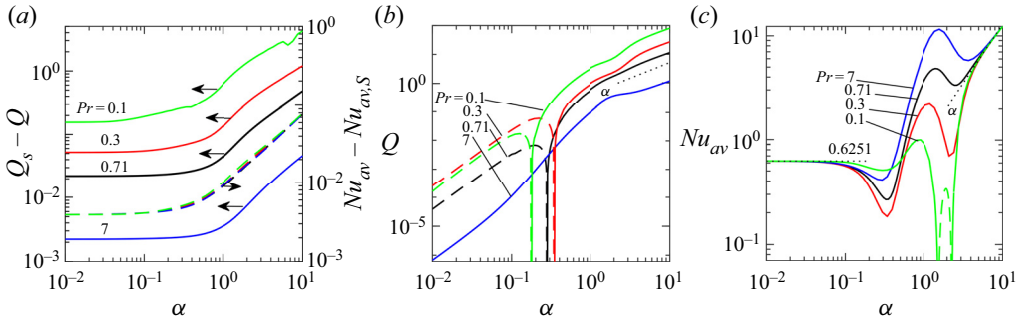


Figure 19. The effect on the flow characteristics induced by changes in the Prandtl number Pr . (a) Variations in Q and Nu_{av} as functions of the groove wavenumber α when $A = 0.05$, $Ra_{uni} = 100$, $Ra_{p,R} = 0$. Dashed lines describe variations of Nu_{av} overlap. (b) Variations in Q as a function of the groove wavenumber α when $A = 0.05$, $\Omega = 0$, $Ra_{p,R} = 400$, $Ra_{uni} = 0$, $\Omega = 0$ and $Pr = 0.1, 0.3, 0.71, 7$ (green, red, black, blue lines, respectively); dashed lines identify change of direction. (c) Variations of Nu_{av} for the same conditions as in (b).

6. Analysis of flow in a grooved slot

We now attempt to throw light on some of the numerical results described in the preceding sections. We comment that, while it is relatively straightforward to describe the flow patterning in the case of a flat walled slot, the presence of the wavy grooves leads to some unfortunate complications. Foremost among these is the fact that grooves mean that the equations must be satisfied in a domain of rather complex shape.

There are essentially two ways to proceed. One would be to retain our original system in the (x, y) coordinate system but this can make the enforcement of the boundary conditions somewhat intricate. We therefore choose to transform from the rectangular (x, y) system and introduce the relevant streamwise length scale $X = \alpha x$ and the cross-channel coordinate

$$\eta = 1 + \frac{4(y - 1)}{4 - A \cos X}, \tag{6.1}$$

in terms of this new coordinate the edges are given by $\eta = \pm 1$. Expressed in terms of these new coordinates the various differential operators are given by

$$\frac{\partial}{\partial x} \rightarrow \alpha \left(\frac{\partial}{\partial X} - \frac{A(\eta - 1) \sin X}{4 - A \cos X} \frac{\partial}{\partial \eta} \right), \quad \frac{\partial}{\partial y} \rightarrow \frac{4}{4 - A \cos X} \frac{\partial}{\partial \eta}, \tag{6.2a,b}$$

and

$$\begin{aligned} \nabla^2 \equiv \alpha^2 \left(\frac{\partial^2}{\partial X^2} - \frac{2A(\eta - 1) \sin X}{4 - A \cos X} \frac{\partial^2}{\partial X \partial \eta} + \frac{(\eta - 1)^2 A^2 \sin^2 X}{(4 - A \cos X)^2} \frac{\partial^2}{\partial \eta^2} \right. \\ \left. + \frac{A(\eta - 1)(2A - 4 \cos X - A \cos^2 X)}{(4 - A \cos X)^2} \frac{\partial}{\partial \eta} \right) + \frac{16}{(4 - A \cos X)^2} \frac{\partial^2}{\partial \eta^2}. \end{aligned} \tag{6.2c}$$

These transformations need to be made in the governing system (2.4) but we do not write out the complicated results in the interest of brevity. What is important to emphasize is that in these new coordinates the boundary conditions become

$$u(\eta = 1) = u(\eta = -1) = 0, \quad v(\eta = 1) = v(\eta = -1) = 0, \tag{6.3a,b}$$

together with $\theta(\eta = 1) = 0$ and $\theta(\eta = -1) = Ra_{uni} + \frac{1}{2} Ra_{p,R} \cos(X + \Omega)$.

6.1. Long-wavelength modes

We start with long-wavelength modes with $\alpha \ll 1$. We seek solutions which assume the structure

$$(u_1, v_1, p_1, \theta_1) = \alpha^{-1}(0, 0, \hat{P}_{-1}, 0) + (\hat{U}_0, 0, \hat{P}_0, \hat{\theta}_0) + \alpha(\hat{U}_1, \hat{V}_0, \hat{P}_1, \hat{\theta}_1) + \alpha^2(\hat{U}_2, \hat{V}_1, \hat{P}_2, \hat{\theta}_2) + \dots, \tag{6.4}$$

where all the unknowns are functions of X and η .

The form of cross-mean momentum equation shows that the leading-order pressure term $\hat{P}_{-1} = \hat{P}_{-1}(X)$ and the energy equation lead to

$$\hat{\theta}_0(X, \eta) = \frac{1}{4}(1 - \eta)[2Ra_{uni} + Ra_{p,L} \cos(X + \Omega)]. \tag{6.5}$$

Now the streamwise momentum (2.4b) equation gives that

$$0 = -\frac{d}{dX}\hat{P}_{-1} + \frac{16}{(4 - A \cos X)^2} \frac{\partial^2 \hat{U}_0}{\partial \eta^2} + \frac{1}{4Pr}(1 - \eta)[2Ra_{uni} + Ra_{p,R} \cos(X + \Omega)], \tag{6.6}$$

whose solution subject to $\hat{U}_0(\pm 1) = 0$ is given by

$$\begin{aligned} \hat{U}_0 &= \frac{1}{32}(4 - A \cos X)^2(\eta^2 - 1) \frac{d}{dX}\hat{P}_{-1} \\ &+ \frac{1}{384Pr}[2Ra_{uni} + Ra_{p,R} \cos(X + \Omega)](4 - A \cos X)^2(\eta - 3)(\eta^2 - 1). \end{aligned} \tag{6.7}$$

If we write this solution as

$$\hat{U}_0 = C_0(X)(\eta^2 - 1) + C_1(X)(\eta - 3)(\eta^2 - 1), \tag{6.8}$$

then the leading-order continuity equation

$$\frac{\partial \hat{U}_0}{\partial X} - \frac{A(\eta - 1) \sin X}{4 - A \cos X} \frac{\partial \hat{U}_0}{\partial \eta} + \frac{4}{4 - A \cos X} \frac{\partial \hat{V}_0}{\partial \eta} = 0, \tag{6.9}$$

may be integrated once. The solution for \hat{V}_0 that vanishes at $\eta = 1$ is

$$\begin{aligned} \hat{V}_0 &= \frac{1}{4}(4 - A \cos X) \left[\frac{dC_0}{dX} \left(\eta - \frac{1}{3}\eta^3 - \frac{2}{3} \right) + \frac{dC_1}{dX} \left(-3\eta + \frac{1}{2}\eta^2 + \eta^3 - \frac{1}{4}\eta^4 + \frac{7}{4} \right) \right] \\ &+ \frac{1}{4}A \sin X \left[C_0 \left(\eta^2 - \frac{2}{3}\eta^3 - \frac{1}{3} \right) + C_1 \left(-\eta - \frac{5}{2}\eta^2 + 3\eta^3 - \frac{3}{4}\eta^4 + \frac{5}{4} \right) \right]; \end{aligned} \tag{6.10}$$

the fact that this must also vanish at $\eta = -1$ furnishes a differential constraint on the functions $C_0(X)$ and $C_1(X)$. This equation can be integrated to deduce that

$$(4 - A \cos X)(C_0 - 3C_1) = K, \tag{6.11}$$

for some constant K to be determined. This result can be rearranged to give

$$\frac{d}{dX}\hat{P}_{-1} = \frac{32K}{(4 - A \cos X)^3} + \frac{1}{4Pr}[2Ra_{uni} + Ra_{p,R} \cos(X + \Omega)]. \tag{6.12}$$

The constant K is set by ensuring that there is no externally imposed pressure gradient. In terms of X and η the requirement that $\partial p/\partial x$ has a zero mean component implies that

$$\int_0^{2\pi} \frac{d}{dX} \hat{P}_{-1} dX = 0. \tag{6.13}$$

Now contour integration gives the result that

$$\int_0^{2\pi} \frac{dX}{(4 - A \cos X)^3} = \frac{\pi(32 + A^2)}{(16 - A^2)^{5/2}}, \tag{6.14}$$

whereupon, on integrating the expression (6.12) over a period, it follows that

$$K = -\frac{Ra_{uni}(16 - A^2)^{5/2}}{32Pr(32 + A^2)}. \tag{6.15}$$

Notice that, in the case of purely periodic heating, this constant is zero. We can also look at the flow rate

$$Q = \int_{y_R(x)}^1 u dy = \frac{1}{4}(4 - A \cos X) \int_{-1}^1 \hat{U}_0 d\eta; \tag{6.16}$$

routine work yields the result that, at leading order,

$$Q = -\frac{1}{3}K = \frac{Ra_{uni}(16 - A^2)^{5/2}}{96Pr(32 + A^2)}. \tag{6.17}$$

To evaluate the mean Nusselt number let us look at the left-hand plate and observe that, there,

$$\frac{\partial \hat{\theta}_0}{\partial y} = \frac{4}{4 - A \cos X} \frac{\partial \hat{\theta}_0}{\partial \eta} = -\frac{2Ra_{uni}}{4 - A \cos X} - \frac{Ra_{p,R} \cos(X + \Omega)}{4 - A \cos X}. \tag{6.18}$$

The mean value of this function taken over a period in X is then given by

$$Nu_{av} = \frac{2Ra_{uni}}{\sqrt{16 - A^2}} + \frac{Ra_{p,R}}{A} \left[\frac{4}{\sqrt{16 - A^2}} - 1 \right] \cos \Omega. \tag{6.19}$$

We can now make some observations about the results (6.17) and (6.19). One immediate conclusion to be drawn is that the mass flux seems to be independent of the periodic component of heating. When there is only uniform heating the formula (6.17) implies that $Q_S - Q = 0.022$ when $Ra_{uni} = 100$ and $A = 0.05$; this is in excellent agreement with the small α solution shown in figure 2(b). When there is only periodic heating the results shown in figure 8(c) suggest that $Q \propto \alpha^2$ as $\alpha \rightarrow 0$, which confirms that the leading-order value should vanish. We point out that it is theoretically possible to develop further terms in (6.4) so as to determine the first non-zero term in the flow rate expansion for small α when $Ra_{uni} = 0$, but this turns out to be a formidable challenge. Last, we also mention that the results in figure 16(a) lend further credence to the conclusion that $Ra_{p,R}$ plays no part in the leading-order mass flux; here, it is seen that the small α limit gives a value of Q independent of the value of this parameter.

Next, we comment on the form of the heat transfer measure Nu_{av} . When $Ra_{p,R} = 0$ and $A = 0.05$ the formula (6.19) shows excellent agreement with the small α limit in figure 2(b). Notice also that the periodic heating does have an $O(1)$ effect on the mean

Nusselt number so long as the phase is such that $\cos \Omega \neq 0$. We can see evidence of this effect in [figure 8\(d\)](#), where the value of Nu_{av} appears to vanish as $\Omega \rightarrow \pi/2$ or $\Omega \rightarrow 3\pi/2$. Moreover, there is excellent agreement between the prediction [\(6.19\)](#) and the $\alpha \rightarrow 0$ limit in [figure 8\(f\)](#). Again, the results in [figure 16\(b\)](#) demonstrate that Nu_{av} depends both on the value of $Ra_{p,R}$ and the phase angle Ω .

It may be hoped that further asymptotic results could be derived in other suitable limits. We alluded, when discussing the results of [figure 5](#), to the fact that large α modes are confined to a thin boundary layer next to the periodically heated flat right-hand wall. Once grooves are introduced the flow structure becomes extremely intricate. Rather than attempt to probe the niceties of the relevant structures, we pursue a rather heuristic argument. We point out that when $\alpha \gg 1$ the rapidly oscillating grooves act as a roughness next to a slot of effective width $1 - (A/2)$. If we approximate this large wavenumber limit by the smooth slot counterparts of results [\(3.1\)](#) for this narrowed slot, then we obtain good agreement with the numerical results at large α .

We might also attempt to describe the flow in a suitable small-amplitude groove limit. Again, it turns out that this approach leads to another very lengthy calculation whose solution requires an effort that is not commensurate with the value of the results. We know the exact flow solution relating to a slot with flat walls and a uniform applied heating (but not periodic heating). When the groove amplitude is small the correction to the solution is given by a problem which can only be solved via the numerical solution of high-order ordinary differential equations with coefficients that are polynomials of high degree.

7. Discussion

Natural convection in vertical slots has been investigated with the aim of assessing the effects of heating and topography patterns and exploring their possible interactions. Topography patterns have been modelled by sinusoidal grooves parametrized by wavenumber and amplitude while heating patterns have been represented by sinusoidal temperature variations. The model equations have been solved with spectral accuracy using a discretization based on Fourier expansions in the vertical direction and Chebyshev expansions in the transverse direction. All the flows have been assumed to be laminar in character.

It has been shown that the addition of grooves to an isothermal plate leads to a reduction in the vertical flow rate and an increase in the transverse heat flow; we conclude that grooves act in a similar way as would a surface roughness. They reduce the effective slot opening, thereby increasing hydraulic resistance and restricting the thermal resistance. Exposing the right plate to a sinusoidal heating while keeping it smooth led to a convection pattern characterized by counter-rotating rolls with no net vertical flow. This convective fluid movement increased the transverse heat flow.

The addition of grooves to a sinusoidally heated plate results in a flow pattern that involves both rolls and stream tubes that carry the fluid vertically. This flow was driven by an interaction effect and the direction of the movement is determined by the relative positions of the heating and the corrugations; overlapping hot spots with groove peaks produce upward flow. An increase in the controlling wavenumber eventually suppresses and then extinguishes the interaction effect; then the grooves play the role of a surface roughness, and the plate behaves either as a hot or cold plate depending on the alignment of the heating and the topography. The addition of a sufficiently large discrepancy between the mean temperature of the two plates produces convection that is dominated by the uniform heating, which disperses the pattern interaction effect with the flow being akin to that found in the case of an isothermal grooved plate.




What we have presented here is very much a first investigation of pattern effects in laminar vertical natural convection that results from a combination of relatively simple thermal and corrugation effects. It would be of interest to extend the scope of the work to determine whether more intricate driving functions might be capable of producing other forms for the convection. Also, it is known that laminar convection easily bifurcates to secondary forms so stability characteristics of various solutions need to be determined and characteristics of various possible secondary flows need to be investigated. These are topics that are under active investigation.

Acknowledgements. The referees are thanked for numerous helpful comments that led to a much improved manuscript.

Funding. This work has been carried out with support from NSERC of Canada.

Declaration of Interests. The authors report no conflict of interest.

Author ORCIDs.

-  J.M. Floryan <https://orcid.org/0000-0003-3296-4122>;
-  S. Panday <https://orcid.org/0000-0001-7120-683X>;
-  Andrew P. Bassom <https://orcid.org/0000-0003-3275-7801>.

REFERENCES

- ABTAHI, A. & FLORYAN, J.M. 2017*a* Natural convection in a corrugated slot. *J. Fluid Mech.* **815**, 537–569.
- ABTAHI, A. & FLORYAN, J.M. 2017*b* Natural convection and thermal drift. *J. Fluid Mech.* **826**, 553–582.
- ABTAHI, A. & FLORYAN, J.M. 2017*c* Convective heat transfer in non-uniformly heated corrugated slots. *Phys. Fluids* **29**, 103605.
- ABTAHI, A. & FLORYAN, J.M. 2018 On the formation of thermal drift. *Phys. Fluids* **30**, 043602.
- ANDREOZZI, A., BUONOMO, B. & MANCA, O. 2005 Numerical study of natural convection in vertical channels with adiabatic extensions downstream. *Numer. Heat Transfer A: Appl.* **47**, 741–762.
- BATCHELOR, G.K. 1954 Heat transfer by free convection across a closed cavity between vertical boundaries at different temperatures. *Q. Appl. Maths* **XII**, 209–233.
- BÉNARD, H. 1900 Les Tourbillons Cellulaires dans une Nappe Liquide. *Revue Gen. Sci. Pure Appl.* **11**, 1261–1271.
- FLORYAN, D. & FLORYAN, J.M. 2015 Drag reduction in heated channels. *J. Fluid Mech.* **765**, 353–395.
- FLORYAN, J.M. & INASAWA, A. 2021 Pattern interaction effect. *Sci. Rep.* **11**, 14573.
- FLORYAN, J.M., SHADMAN, S. & HOSSAIN, M.Z. 2018 Heating-induced drag reduction in relative movement of parallel plates. *Phys. Rev. Fluids* **3**, 094102.
- HALL, P. 2012 Vortex-wave interactions: long wavelength streaks and spatial localization in natural convection. *J. Fluid Mech.* **703**, 99–110.
- HOSSAIN, M.Z. & FLORYAN, J.M. 2013 Instabilities of natural convection in a periodically heated layer. *J. Fluid Mech.* **733**, 33–67.
- HOSSAIN, M.Z. & FLORYAN, J.M. 2014 Natural convection in a fluid layer periodically heated from above. *Phys. Rev. E* **90**, 023015.
- HOSSAIN, M.Z. & FLORYAN, J.M. 2015*a* Mixed convection in a periodically heated channel. *J. Fluid Mech.* **768**, 51–90.
- HOSSAIN, M.Z. & FLORYAN, J.M. 2015*b* Natural convection in a horizontal fluid layer periodically heated from above and below. *Phys. Rev. E* **92**, 023015.
- HOSSAIN, M.Z. & FLORYAN, J.M. 2016 Drag reduction in a thermally modulated channel. *J. Fluid Mech.* **791**, 122–153.
- HOSSAIN, M.Z. & FLORYAN, J.M. 2020 On the role of surface grooves in the reduction of pressure losses in heated channels. *Phys. Fluids* **32**, 083610.
- HOSSAIN, M.Z., FLORYAN, D. & FLORYAN, J.M. 2012 Drag reduction due to spatial thermal modulations. *J. Fluid Mech.* **713**, 398–419.
- HUGHES, G.O. & GRIFFITHS, R.W. 2008 Horizontal convection. *Annu. Rev. Fluid Mech.* **40**, 185–208.
- HUSAIN, S.Z. & FLORYAN, J.M. 2010 Spectrally-accurate algorithm for moving boundary problems for the Navier-Stokes equations. *J. Comput. Phys.* **229**, 2287–2313.

- HUSAIN, S.Z., SZUMBARSKI, J. & FLORYAN, J.M. 2009 Over-determined formulation of the immersed boundary condition method. *Comput. Meth. Appl. Mech. Engng* **199**, 94–112.
- INASAWA, A., HARA, K. & FLORYAN, J.M. 2021 Experiments on thermal drift. *Phys. Fluids* **33**, 087116.
- JIANG, H., ZHU, X., MATHAI, V., YANG, X., VERZICCO, R., LOHSE, D. & SUN, C. 2019 Convective heat transfer along ratchet surfaces in vertical natural convection. *J. Fluid Mech.* **873**, 1055–1071.
- LEE, Y. & KORPELA, S.A. 1983 Multicellular natural convection in a vertical slot. *J. Fluid Mech.* **126**, 91–121.
- LINDEN, P.F. 1999 The fluid mechanics and natural ventilation. *Annu. Rev. Fluid Mech.* **31**, 201–38.
- MOHAMMADI, A. & FLORYAN, J.M. 2013 Pressure losses in grooved channels. *J. Fluid Mech.* **725**, 23–54.
- NAGLER, J. 2021 Numerical simulation of a mixed vertical ventilation system. *Z. Angew. Math. Mech.* **101**, e201900353.
- NAYLOR, D., FLORYAN, J.M. & TARASUK, J.D. 1991 A numerical study of developing free convection between isothermal vertical plates. *Trans. ASME J. Heat Transfer* **113**, 620–626.
- NG, C.S., OOI, A., LOHSE, D. & CHUNG, D. 2015 Vertical natural convection: application of the unifying theory of thermal convection. *J. Fluid Mech.* **764**, 349–361.
- NOVAK, M. & FLORYAN, J.M. 1995 Free convection in systems of vertical channels. *Intl J. Heat Fluid Flow* **16**, 244–253.
- PUTNAM, J.O. 1882 *The Open Fire for All Ages*. James R. Osgood and Company.
- RAYLEIGH, LORD 1916 On convection currents in a horizontal layer of fluid, when the higher temperature is on the under side. *Phil. Mag.* **32**, 529–546.
- SHAHIN, G.A. & FLORYAN, J.M. 1999 Heat transfer enhancement generated by the chimney effect in systems of vertical channels. *Trans. ASME J. Heat Transfer* **121**, 230–232.
- SHISHKINA, O. & WAGNER, C. 2011 Modelling the influence of wall roughness on heat transfer in thermal convection. *J. Fluid Mech.* **686**, 568–582.
- SONG, Z., HUANG, X., KUENZER, C., ZHU, H., JIANG, J., PAN, X. & ZHONG, F. 2020 Chimney effect induced by smoldering fire in a U-shaped porous channel: a governing mechanism of the persistent underground coal fires. *Process Saf. Environ. Prot.* **136**, 136–147.
- STRAATMAN, A.G., NAYLOR, D., TARASUK, J.D. & FLORYAN, J.M. 1994 Free convection between inclined isothermal plates. *Trans. ASME J. Heat Transfer* **116**, 243–245.
- STRAATMAN, A.G., TARASUK, J.D. & FLORYAN, J.M. 1993 Heat transfer enhancement from a vertical, isothermal channel generated by the chimney effect. *Trans. ASME J. Heat Transfer* **115**, 395–402.
- SZUMBARSKI, J. & FLORYAN, J.M. 1999 A direct spectral method for determination of flows over corrugated boundaries. *J. Comput. Phys.* **153**, 378–402.
- TOPPALADODDI, S., SUCCI, S. & WETTLAUFER, J.S. 2017 Roughness as a route to the ultimate regime of thermal convection. *Phys. Rev. Lett.* **118**, 074503.
- TOURNIER, C., GETHON, P. & RABINOWICZ, M. 2000 The onset of natural convection in vertical fault planes: consequences for the thermal regime in crystalline basements and for heat recovery experiments. *Geophys. J. Intl* **140**, 500–508.
- VEST, C.M. & ARPACI, V.S. 1969 Stability of natural convection in a vertical slot. *J. Fluid Mech.* **36**, 1–15.
- WEIL, A. (Ed.) 2012 *Nuclear Power. Practical Aspects*. IntechOpen Book Series. ISBN: 978-953-51-0778-1.
- WONG, N.H. & HERYANTO, S. 2004 The study of active stack effect to enhance natural ventilation using wind tunnel and computational fluid dynamics (CFD) simulations. *Energy Build.* **36**, 668–678.
- ZELDOVICH, Y.B. 1937 Limiting laws of freely rising convection currents. *Zh. Eksp. Teor. Fiz.* **7**, 1463–1465.